RSC Advances

PAPER

View Article Online
View Journal | View Issue

Cite this: *RSC Adv.*, 2014, **4**, 12078

f-Orbital covalency in the actinocenes (An = Th–Cm): multiconfigurational studies and topological analysis†

Andrew Kerridge*

Received 27th November 2013
Accepted 17th February 2014

DOI: 10.1039/c3ra47088a

www.rsc.org/advances

The CASSCF methodology is used to calculate the ground state electron densities of a series of seven actinocenes, $AnCOT_2$ (An = Th–Cm, COT = η^8-C_8H_8). The multiconfigurational character of these complexes is found to be substantial and topological analysis of the electron density *via* the QTAIM approach is therefore chosen in order to investigate the electronic structure in more detail. Topological analysis reveals increased values of the electron density at the An–C bond critical point for An = Pa–Pu, suggesting enhanced covalent character in metal–ligand bonding for these complexes. In order to investigate the origins of this covalency, integrated one- and two-electron properties are evaluated. A trend for increased electronic charge, spin density and electron localisation on the An centre as one traverses the actinide series is found. The difference between atomic number and the electron localisation index is considered and found to correlate well with the expected oxidation state in these complexes, with a tendency towards trivalent character for the later actinides. Total and orbitally resolved delocalisation indices are evaluated, and increased electron delocalisation is found for the complexes containing Pa–Pu centres. It is shown that, while 5f contributions to covalency in these complexes are smaller in magnitude than 6d contributions, the *variation* in covalency is almost entirely accounted for by the variation in the 5f contribution.

Introduction

The quantification of covalency in f-element complexes is of both fundamental scientific interest and critical industrial importance. In the nuclear power industry, the remediation of spent nuclear fuel is based on the chemical separation of minor actinides from lanthanides.[1,2] That this separation is possible is believed to be due to the more radially extended nature of the 5f shell of the former, resulting in enhanced covalent interactions with soft donor ligands[3] when compared to those of the latter, which are characterised by a contracted, core-like, 4f shell. Advantage can be taken of the stability afforded by this enhanced covalent interaction in order to design ligands which are strongly selective for actinides over lanthanides,[1,4] from which separation processes follow. The presence of strong electron correlation, however, makes metal–ligand covalency difficult to quantify in complexes containing open shell ions.[5,6] Whilst the identification of near-degeneracy between actinide 5f and carbon 2p orbitals in a variety of complexes[7,8] has shown promise in developing our understanding of the role of the 5f orbitals in bonding, static correlation, manifesting itself in the form of multiconfigurational character in the electronic wavefunction, results in the failure of these traditional views of covalency due to the breakdown of the independent particle approximation. In order to allow the question of covalency in such multiconfigurational systems to be considered, one can instead turn to the physically observable total electron density. When this is taken as the fundamental property to be analysed, advantage can be taken of topological analysis through the application of the quantum theory of atoms in molecules[9] (QTAIM), which allows for the decomposition of a molecule into a space-filling and contiguous set of open quantum systems, or 'atomic basins'. This topological analysis can be used to infer details of the nature of bonding interactions within the system of interest and can be extended to also consider integrated one- and two-electron properties.

Computational chemical approaches are established as important tools in developing our understanding of fundamental actinide chemistry[10] and in this work, the covalent contribution to bonding in the prototypical actinide organometallic sandwich complexes, $AnCOT_2$ (COT = η^8-C_8H_8), is investigated. Since the first synthesis of uranocene ($UCOT_2$) was reported by Streitwieser and Müller-Westerhoff in 1968,[11] a significant amount of effort has been expended by the actinide chemistry community in order to elucidate the chemical properties of the actinocenes. In addition to uranocene, a number of other $AnCOT_2$ (An = Th, Pa, Np, Pu, Am) complexes have been

Department of Chemistry, University College London, 20 Gordon Street, London, WC1H 0AJ, UK. E-mail: a.kerridge@ucl.ac.uk

† Electronic supplementary information (ESI) available. See DOI: 10.1039/c3ra47088a

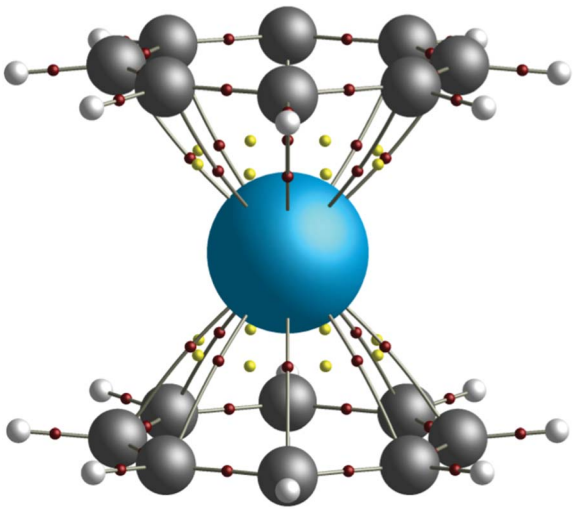

Fig. 1 QTAIM calculated molecular graph of the D_{8h} symmetry thorocene complex, $ThCOT_2$. Bond critical points (BCPs) are shown in red, ring critical points (RCPs) in yellow.

synthesised,[12–15] the latter as the trivalent potassium salt. Whilst there is a significant body of experimental literature relating to the actinocenes, the high (D_{8h}) symmetry of these complexes (see Fig. 1) has made them particularly amenable to theoretical studies, which have demonstrated the need for a multi-configurational description of the wavefunction.[16–22] Here, electron densities derived from complete-active-space self-consistent-field (CASSCF) calculations are used as the basis for topological investigations using QTAIM. A trend in covalency is established across the series, indicating maximum covalent character in the U, Np and Pu complexes. Novel analysis based on the orbital decomposition of integrated electronic properties is employed in order to show that although actinide 5f orbital contributions to covalent character are *not* the dominant contributions in these complexes, the variation in covalency found across the series *is* commensurate with the variation in An 5f contributions.

Computational details

Complete-active-space self-consistent-field (CASSCF)[23] calculations were performed using version 7.6 of the MOLCAS quantum-chemical software package.[24,25] Throughout, ANO-RCC basis sets of polarised triple-zeta quality were used.[26–28] Molecular geometries were obtained by optimising the distance between the An ion and the ring centroid of the COT dianion with respect to complete active space second order perturbation theory (CASPT2)[29] calculated energies. In all calculations, the geometric structure of the COT ligand was held at the geometry used in previous studies.[18,20–22] CASPT2 calculations employed an imaginary level shifting technique in order to minimise the effect of intruder states. The value of this level shift was 0.2. Topological analysis employing QTAIM was performed using the AIMAll[30] and Multiwfn[31] codes. Whilst there are numerous examples in the literature of other analytical approaches, such as Mulliken, NBO or energy decomposition analysis, being used in attempts to deepen our understanding of bonding in f-element complexes, such approaches have not been employed in this study. Mulliken analysis is well known as providing only a qualitative description of atomic populations in actinide complexes,[32] whereas NBO and energy decomposition approaches can give somewhat contradictory results when applied to the question of covalency.[33] While QTAIM is, like any approach, open to a degree of interpretation, previous work has shown it to be a robust tool in the analysis of f-block compounds, exhibiting trends commensurate with chemical intuition.[6,22] QTAIM also has the advantage of being easily applicable to multi-configurational systems, and it has therefore been chosen as the method of analysis employed in this study.

Although all complexes considered here possess D_{8h} point group symmetry, restrictions of the MOLCAS code require that calculations were performed using its highest abelian subgroup, D_{2h}. Bearing this in mind, irreducible representations (irreps) of D_{2h} will be used in the discussion.

Throughout the bonding analysis performed in this study, the effects of dynamical correlation and spin-orbit coupling (SOC) are neglected. Whilst the former could be included *via* multi-configurational second-order perturbation theory (*e.g. via* the CASPT2 approach employed in the geometry optimisations) and the latter *via* the restricted-active space state interaction (RASSI) approach, it was not possible to generate total electron densities in a manner amenable to QTAIM analysis. Inclusion of dynamical correlation effects would not be expected to significantly affect the results presented here since the important electron interactions associated with the bonding between ion and ligand are incorporated within the chosen active spaces: all electrons included in the active spaces are explicitly correlated. Whilst the effects of SOC can be significant in actinide complexes, they are again expected to have little effect on bonding character. It has previously been shown[21] that although the effects of SOC on the energetics of $UCOT_2$ and $PuCOT_2$ are pronounced, they have virtually no effect on the calculated geometries of these complexes, implying little effect on the character of the bonding interaction. This is unsurprising since, within the RASSI formalism, SOC states are constructed from a basis of CASSCF-states calculated in the absence of SOC, and the CASSCF basis states only differ in the occupation of non-bonding 5f-orbitals.

Active spaces

In all $AnCOT_2$ calculations, a 16 orbital active space was constructed, as used previously.[22] This active space incorporates the highest occupied π-orbitals of a_u, b_{1u}, a_g and b_{1g} symmetry (in keeping with previous work[18,20–22]) along with the seven f-orbitals of a_u (f_δ), b_{1u} (f_σ, f_δ), b_{2u} (f_π, f_φ) and b_{3u} (f_π, f_φ) symmetry and the five d-orbitals of a_g (d_σ, d_δ), b_{1g} (d_δ), b_{2g} (d_π) and b_{3g} (d_π) symmetry. Adopting the CASSCF(n, m) notation to indicate a calculation incorporating an active space explicitly correlating n electrons in m orbitals, this selection results in CASSCF(n, 16) calculations, with n ranging from 8 (Th) to 14 (Cm).

Results

Geometry optimisations

For each complex, the electronic ground state was identified by evaluating the CASPT2-calculated energy of the lowest lying state of each of the eight irreducible representations of the D_{2h} point group. Ground state total energies were then calculated at a series of ring centroid-metal separations between 1.700 and 2.300 Å. In total, approximately 20 data points were obtained for each complex. These data were fitted with a sixth-order polynomial in order to obtain equilibrium ring-metal separations. The results of these calculations are given in Fig. 2, along with the ground electronic states of each complex. Of the seven complexes considered here only three, $ThCOT_2$, $UCOT_2$ and $NpCOT_2$ have been structurally characterised,[34,35] with experimentally determined ring-metal separations (r_{RM}) of 2.004, 1.926 and 1.909 Å, respectively. The present calculations give optimised r_{RM} of 2.002, 1.907 and 1.890 Å, in good agreement with the experimental data. Table 1 compares r_{RM} with ionic radii (IR) taken from the literature.[36] There is, in general, good agreement between the two, particularly in relation to the significant reduction in both r_{RM} and IR when moving from Th to Pa. As one looks further across the series however, an interesting trend appears: the ratio r_{RM}/IR gradually increases, which may be indicative of increased charge concentration on the An ion and/or a reduction in covalent interaction between ligand and ion. The small increase in r_{RM} of 0.021 Å when comparing $CmCOT_2$ to $AmCOT_2$ may therefore be a manifestation of the same effect, and will be investigated in more detail in the following sections.

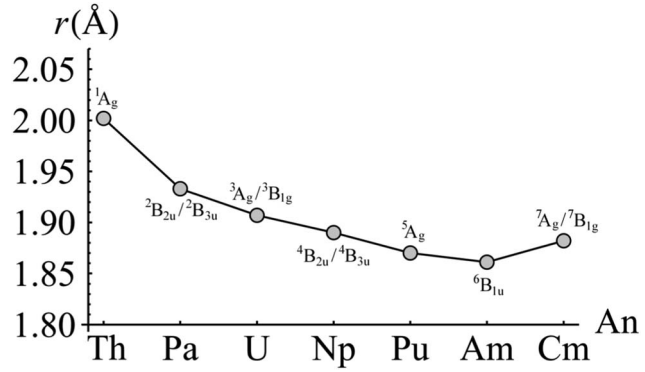

Fig. 2 CASPT2-calculated $AnCOT_2$ ring-metal separations. The electronic state for which the geometry was optimised is indicated above and below the corresponding data point.

Table 1 Comparison of CASPT2-calculated ring-metal separations, r_{RM}, and ionic radii of tetravalent actinide ions,[36] IR

Complex	r_{RM} (Å)	IR (Å)	r_{RM}/IR
$ThCOT_2$	2.002	0.94	2.130
$PaCOT_2$	1.933	0.90	2.148
$UCOT_2$	1.907	0.89	2.143
$NpCOT_2$	1.890	0.87	2.172
$PuCOT_2$	1.870	0.86	2.174
$AmCOT_2$	1.861	0.85	2.189
$CmCOT_2$	1.882	0.85	2.214

Natural orbital analysis

In order to better understand the electronic structure of the metallocenes, the natural spin-orbitals (NOs) and corresponding occupations (NOOs) were evaluated for each complex. The natural orbitals, introduced by Löwdin,[37] are obtained *via* the diagonalisation of the first order reduced density matrix (RDM), and therefore provide an unambiguous orbital decomposition of the electron density. The NOs also have the property that they are maximum-occupancy orbitals and are thus a basis for the most compact CI description of the wavefunction. It follows that, for an electronic state constructed from a monodeterminantal wavefunction, every NOO will take a value of 0, 1 or 2. For a multiconfigurational electronic state, the deviation of the NOOs from integer values can be taken as a measure of multiconfigurational character.[38] Occupation numbers close to integer values correspond to 'strongly' occupied orbitals, whereas occupation numbers close to zero correspond to 'weakly' occupied orbitals.

The D_{8h} point group symmetry and η^8 hapticity of $AnCOT_2$, combined with the fact that the highest lying π-orbitals of the $(COT^{2-})_2$ ligand system span the e_{2g} and e_{2u} irreps,‡ allows for the possible participation of the An $6d_\delta$ (e_{2g} symmetry) and $5f_\delta$ (e_{2u} symmetry) orbitals in delta-type metal–ligand bonding,[14,39–43] respectively. The natural orbital analysis therefore begins with consideration of these orbitals. Bearing in mind that calculations are performed in D_{2h} symmetry, Fig. 3 presents the natural orbitals occupations (NOOs) for the strongly and weakly occupied orbitals of (a) $a_g \oplus b_{1g}$ and (b) $a_u \oplus b_{1u}$ symmetry. Fig. 3a shows that the NOOs corresponding to the *gerade* orbitals show little variation when moving across the actinide series and are very closer to integer values. The strongly occupied orbitals have NOOs ranging from 3.904 ($ThCOT_2$) to 3.964 ($CmCOT_2$) whilst the weakly occupied orbitals have NOOS ranging from 0.024 ($ThCOT_2$) to 0.040 ($PuCOT_2$). These NOOs indicate a degree of multiconfigurational character and justify the inclusion of these orbitals in the active spaces employed here. Visualisation of the orbitals reveals a degree of metal–ligand hybridisation, with the strongly (weakly) occupied orbitals exhibiting bonding (antibonding) character: the question of whether this corresponds to An 6d covalency will be considered in later sections. Fig. 3b presents the corresponding data for the *ungerade* orbitals. Here, a more pronounced trend is apparent. There is a reduction in the occupation of the strongly occupied orbitals when moving across the series from Th (3.896) to Am (3.652), along with a concomitant increase in occupation of the weakly occupied orbitals, 0.016 for $ThCOT_2$, 0.340 for $AmCOT_2$. This trend has been reported previously for a subset of the complexes considered here[21] and indicates a degree of multiconfigurational character in $PuCOT_2$ and $AmCOT_2$ comparable to that previously reported in several related Ce complexes.[20,44,45]

‡ In the subduction from D_{8h} to (the working symmetry) D_{2h}, $e_{2g/2u} \rightarrow a_{g/u} \oplus b_{1g/1u}$.

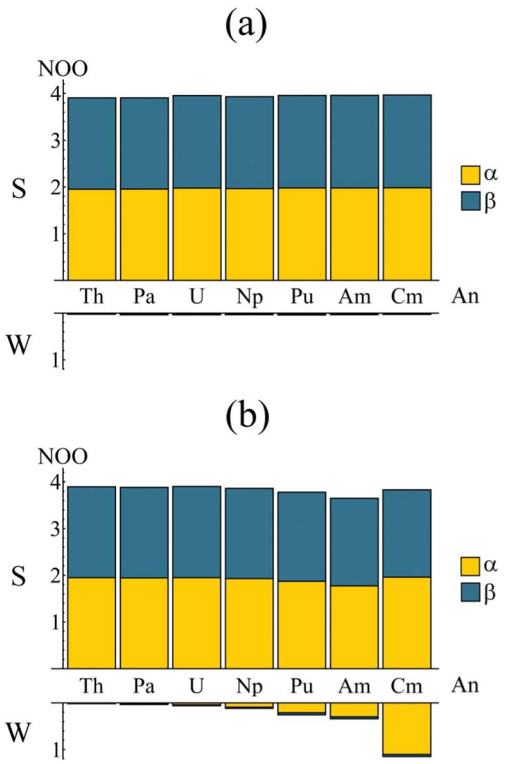

Fig. 3 Natural orbital occupations of the strongly (S) and weakly (W) occupied orbitals of (a) a_g/b_{1g} symmetry and (b) a_u/b_{1u} symmetry. Occupations are summed since in the full (D_{8h}) symmetry of the complexes considered here $a_{g/u} \oplus b_{1g/1u}$ spans $e_{2g/2u}$. See Table S1† for numerical data.

Fig. 3b shows almost equal spin-up (α) and spin-down (β) occupation of the strongly occupied a_u/b_{1u} natural orbitals, mirroring the a_g/b_{1g} orbital occupations presented in Fig. 3a. The weakly occupied a_u/b_{1u} orbitals, however, exhibit a strong preference for occupation of the α-orbital, increasing the spin density associated with the $5f^n$ occupation of the An ions.

Whilst the trend from Th–Am is quite clear, there is a marked deviation between the Am and Cm complexes. The trend towards lower occupations of the strongly occupied a_u/b_{1u} orbitals is reversed in the latter, with an occupation of 3.832 being comparable to that of the early actinide complexes. There is also a substantial increase in occupation of the weakly occupied a_u/b_{1u} orbitals (1.149 compared to 0.340 in $AmCOT_2$). This is, however, to be expected. Whilst the An $5f_\delta$ orbitals form (anti-)bonding linear combinations with the ligand π_{2u} HOMO, the $5f_\sigma$, $5f_\pi$ and $5f_\phi$ orbitals are essentially non-bonding. These non-bonding orbitals become fully occupied in the $5f^5$ Am complex and so the $5f^6$ configuration of $CmCOT_2$ must, by necessity, involve occupation of the energetically unfavourable antibonding π_{2u}–$5f_\delta$ orbital: this corresponds to the NOO of the 'weakly' occupied orbital of Fig. 3b. The occupation of this antibonding orbital is commensurate with the increased ring-metal separation of $CmCOT_2$ over $AmCOT_2$. Furthermore, the occupation number of 3.832 found in $CmCOT_2$ has the same origin. Since only one antibonding orbital is now available for (weak) occupation, so only one strongly occupied orbital has a commensurate reduced occupation number. Since the value of 3.832 is in fact the sum of occupations of two orbitals it is, as expected, higher than that of the other later actinides considered here.

Table 2 Natural orbital occupations of the non-bonding 5f orbitals of all complexes considered in this study. $5f_{NB}$ gives the total occupation of non-bonding 5f orbitals

Complex	Configuration	$5f_\sigma$	$5f_\pi$	$5f_\phi$	$5f_{NB}$
$ThCOT_2$	$5f^0$	—	—	—	0
$PaCOT_2$	$5f^1_\phi$	—	—	0.980	0.980
$UCOT_2$	$5f^1_\pi5f^1_\phi$	—	0.995	0.993	1.988
$NpCOT_2$	$5f^2_\pi5f^1_\phi$	—	1.956	0.982	2.938
$PuCOT_2$	$5f^2_\pi5f^2_\phi$	—	1.946	1.924	3.870
$AmCOT_2$	$5f^1_\sigma5f^2_\pi5f^2_\phi$	0.983	1.972	1.962	4.917
$CmCOT_2$	$5f^1_\sigma5f^2_\pi5f^1_\delta5f^2_\phi$	0.984	1.969	1.969	4.922

Finally, the An non-bonding 5f NOOs are given in Table 2. From these, the leading $5f^n$ configurations can be derived, indicating a preference for occupation of the (presumably near-degenerate) $5f_\pi$ and $5f_\phi$ orbitals over occupation of $5f_\sigma$. The degree to which these orbitals can be considered as non-bonding and localised on the An centre will be discussed later in this study. As would be expected, the total non-bonding 5f orbital occupation increases by approximately integer amounts as the actinide series is crossed.

Topological analysis

As previously discussed, the strong static correlation present in the complexes under consideration (as evidenced by the increasing NOOs of the weakly occupied orbitals of a_u/b_{1u} symmetry highlighted in Fig. 3b) makes covalency measures based on orbital mixing due to energetic near-degeneracy at best ambiguous. As an alternative, the total electron density can be investigated by employing the Quantum Theory of Atoms in Molecules (QTAIM). The topological analysis afforded by this approach allows for a molecule to be divided into a contiguous set of space-filling atomic basins, the surfaces of which satisfy the condition $\nabla\rho(r)\cdot n(r) = 0$. Evaluation of $\nabla\rho(r) = 0$ reveals the set of critical points associated with the molecule. Each atomic basin (typically) contains a single nuclear critical point (NCP) at the position of the nuclear centre. A bond critical point (BCP) is found when the uniquely defined line of maximum density between two atoms has its minimum at the interatomic surface joining the two atomic basins: in this situation, the atoms are considered to be bonded to one another.[46] The nature of this bonding can be characterised by the values of the density and its Laplacian at the BCP: as a general rule, $\rho_{BCP} > 0.20$ a.u. and $\nabla^2\rho_{BCP} < 0$ for a covalent bond, whilst $\rho_{BCP} < 0.10$ a.u. and $\nabla^2\rho_{BCP} > 0$ indicates an ionic bond. More broadly, increasing values of ρ_{BCP} indicate increasing covalent character of the bonding interaction.

Fig. 4 shows the value of ρ_{BCP} and its Laplacian at the metal–carbon critical point for each complex considered here. Values of ρ_{BCP} are ~0.04 a.u., with the Laplacian being small and positive in all cases. This is indicative of a predominantly ionic interaction, as would be expected. However, whilst the

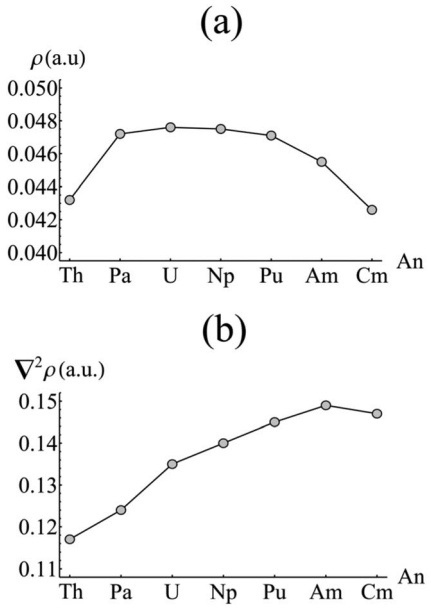

Fig. 4 Values of (a) the electron density (ρ) and (b) its Laplacian ($\nabla^2\rho$) evaluated at the metal–carbon bond critical point in $AnCOT_2$ (An = Th–Cm). See Table S2† for numerical data.

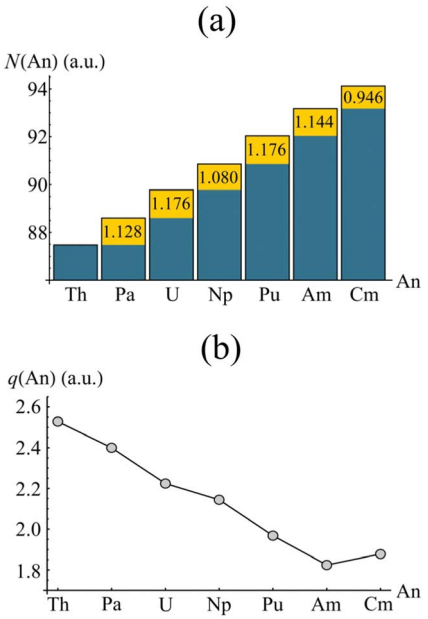

Fig. 5 QTAIM calculated atomic populations (a) and atomic charges (b) of the An centres in $AnCOT_2$ (An = Th–Cm). The yellow regions in (a) show the increase of electron density in Ω_{An} when compared to the previous element. See Table S3† for numerical data.

Laplacian slowly increases across the series from Th–Am (with a small reduction upon moving to Cm), the density itself exhibits a pronounced maximum between Pa and Pu, with a maximum value of $\rho_{BCP} = 0.476$ a.u. found in $UCOT_2$. This suggests that the early actinides, with the exception of Th, exhibit a more covalent interaction with the COT ligand than those occurring later in the series. The low value associated with the formally $5f^0$ thorium complex may indicate the involvement of the $5f_\delta$ orbitals in the covalent interaction of the other complexes. Moreover, the maximum value found in $UCOT_2$ is consistent with the results obtained from density functional theoretical studies of $AnCp_3$.[47]

Integrated one- and two-electron properties

Whilst the topological analysis discussed in the previous section suggests enhanced covalency amongst the Pa, U, Np and Pu actinocenes, more detailed information is required in order to identify its origin. The atomic basins identified previously can again be employed. Integrating the electron density over an atomic basin Ω_A gives the atomic population N(A) from which the atomic charge q(A) can be derived. If instead one considers the exchange–correlation component of the electron pair density, two further properties can be defined: the localisation index, λ(A), obtained by integration of both components of the pair density over the same atomic basin Ω_A, and the delocalisation index, δ(A, B), obtained by integrating one component over Ω_A and one over Ω_B. λ(A) corresponds to the average number of electrons localised upon a given atom, while δ(A, B) quantifies the average number of electrons shared between two atoms and can be considered as an unambiguous and quantitative measure of covalency. Formally, the evaluation of two-electron properties requires explicit knowledge of the 2nd order RDM. Construction of this matrix, however, is computationally demanding, and so approximate methods have been developed based on the 1st order RDM. In this work, the approximate form of the 2nd order RDM proposed by Müller[48] is employed.

Fig. 5 shows the atomic populations N(An) and atomic charges q(An) of the metal centre of each complex considered in this study. The element-by-element increase in N(An) is highlighted in yellow. For the elements Pa–Am, this increase is slightly greater than unity, and manifests itself in a steadily decreasing atomic charge, as shown in Fig. 3b. The difference in actinide charge between $ThCOT_2$ to $AmCOT_2$ is 0.704 a.u., evident of strong trivalent character in the latter. This is not unexpected for the later actinides, the chemistry of which bears strong similarities to that of the lanthanides.

The increase in atomic population when moving from Am to Cm deviates from the trend discussed above. Here, the increase is marginally less than unity, resulting in a Cm charge slightly higher than that of Am. As previously discussed, $CmCOT_2$ is the only complex considered here which exhibits occupation of anything other than a nonbonding 5f orbital, namely an antibonding π_{2u}–$5f_\delta$ orbital. The fact that this orbital has a degree of ligand character explains this deviation from the Th–Am trend.

In order to investigate the increased trivalent character suggested by analysis of the atomic charges, the localisation indices λ(An) were evaluated, and are presented in Fig. 6a. Again the element-by-element increase is highlighted in yellow. In each case (except that of Th & Pa), λ(An) increases by an amount greater than unity, this being most pronounced between Np & Pu and Pu & Am. This has a cumulative effect as one traverses the actinide series, as can be seen in Fig. 6b. Here, the difference between the atomic number, Z, and λ(An) is given for An = Th–Cm. λ(An) is a measure of the number of electrons

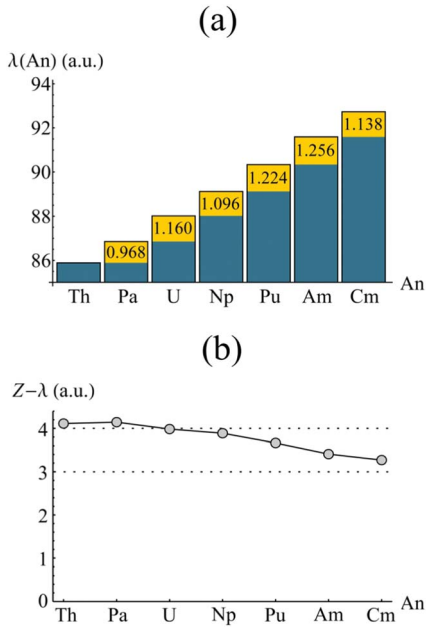

Fig. 6 QTAIM calculated localisation indices (a) and differences between atomic number and λ(An) (b) of the An centres in $AnCOT_2$ (An = Th–Cm). The yellow regions in (a) show the increase of electron localisation in Ω_{An} when compared to the previous element. See Table S4† for numerical data.

localised on An, and so Z(An)–λ(An), which therefore gives the number of electrons donated and/or shared by the An atom, might be expected to give a measure of formal oxidation state. Z(An)–λ(An) ~ +4 for An = Th–Np, mirroring the expected value. For later actinides, however, electron localisation increases: in $CmCOT_2$, Z(Cm)–λ(Cm) = 3.270, implying a trivalent oxidation state. The same assignment can be made for $AmCOT_2$, with $PuCOT_2$ appearing to be best described as mixed valent according to this criterion. This latter conclusion is in accord with previous findings.[22]

Assuming the Müller approximation to the 2nd order RDM, λ(An) and δ(An, C) can be decomposed into orbital contributions:[49]

$$\lambda(\mathrm{An}) = \sum_{i,j}^{\mathrm{NO}} \sqrt{n_i}\sqrt{n_j}\left[S_{ij}(\mathrm{An})\right]^2,$$

$$\delta(\mathrm{An},\mathrm{C}) = \sum_{i,j}^{\mathrm{NO}} \sqrt{n_i}\sqrt{n_j}S_{ij}(\mathrm{An})S_{ij}(\mathrm{C}),$$

where n_i is the NOO of the natural orbital φ_i, S_{ij}(A) is the overlap integral between NOs φ_i and φ_j evaluated over the atomic basin Ω_A, and the summation runs over all NOs. Advantage can be taken of these definitions in order to obtain orbital contributions to electron (de)localisation. In particular, 5f and 6d contributions can be evaluated for the $MCOT_2$ complexes considered in this study. This is possible due to the high symmetry of these complexes. The central atomic basin Ω_{An} will have the same symmetry as the molecule and, since the 5f and 6d have *ungerade* and *gerade* parity, respectively, the overlap integrals $S_{5f,6d}$(An) will be equal to zero. The decomposition of the (de)localisation index into orbital contributions as used in this study is depicted schematically in Fig. 7. In addition to the total (de)localisation indices, the contributions from the π-electron subsystem ($\lambda^{\pi}/\delta^{\pi}$), the $5f_\delta$ and π_{2u} orbitals ($\lambda^{5f_\delta}/\delta^{5f_\delta}$) and the $6d_\delta$ and π_{2g} orbitals ($\lambda^{6d_\delta}/\delta^{6d_\delta}$) are also evaluated.

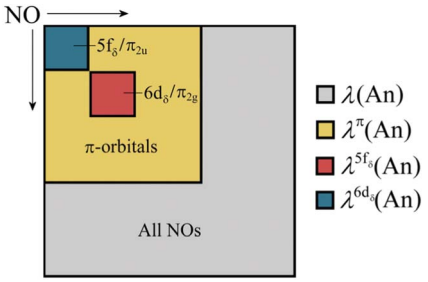

Fig. 7 Schematic showing the various contributions to the orbitally resolved localisation indices evaluated in this study.

Firstly, the π-orbital, $5f_\delta$ and $6d_\delta$ contributions to the localisation index are considered. In the case of the $5f_\delta$ ($6d_\delta$) contribution, the ligand π_{2u} (π_{2g}) orbitals (which are able to mix with the respective metal orbitals) are also included in the summation. Fig. 8a presents the orbitally resolved localisation indices. There is a substantial increase in An localisation amongst the π-electron subsystem as one moves from Th to Am, and this localisation is almost entirely due to increased localisation amongst the $5f_\delta$ and π_{2u} orbitals, with contributions from $6d_\delta$ and π_{2g} orbitals remaining approximately constant across the series. The substantial increase in the case of $CmCOT_2$ is again due to the occupation of the antibonding π_{2u}–$5f_\delta$ orbital. Fig. 8b reveals that the degree of electron localisation amongst the nonbonding 5f orbitals is, as expected, almost total, with localisation indices ranging from 92.0% (Pa) to 98.6% (Cm) of the total nonbonding 5f populations (N(An) in Fig. 8b).

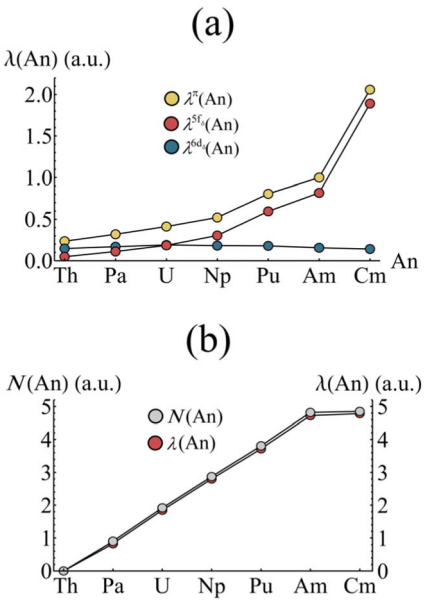

Fig. 8 (a) Orbitally resolved localisation indices and (b) comparison of nonbonding 5f occupation and localisation for $AnCOT_2$ (An = Th–Cm). See Table S5† for numerical data.

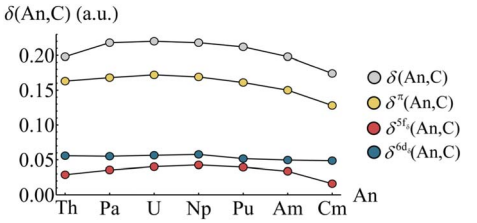

Fig. 9 Total and orbitally resolved delocalisation indices for $AnCOT_2$ (An = Th–Cm). See Table S6† for numerical data.

In order to quantify An–C covalency in these complexes, delocalisation indices δ(An, C) were evaluated in analogy with the orbitally resolved localisation indices. These delocalisation indices are presented in Fig. 9. The trend in total delocalisation index from Th to Cm mirrors the trend in ρ_{BCP} (*cf.* Fig. 2a). As previously discussed, an increase in ρ_{BCP} corresponds to an increase in covalent bonding character and so a commensurate increase in electron delocalisation would be expected. That this increase is found strongly supports the view that there is indeed enhanced covalent character in the complexes of the early actinides, Pa–Pu. Whilst the magnitude of delocalisation indices is quite modest, δ(An, C) taking a maximum value of 0.220 a.u. in $UCOT_2$, it should be borne in mind that this value corresponds to the average number of electrons shared between the An centre and *a single* carbon centre. Since there are sixteen carbons atoms in $AnCOT_2$, the total number of electrons shared is significantly larger and is listed in Table 3.

The trend in delocalisation indices is mirrored by the contribution from the π-electron subsystem, which accounts for approximately 77% of the total value, on average. This implies a not insignificant contribution from NOs with σ-character, although the orbital decomposition here means that contributions from terms involving the overlap integrals $S_{\sigma\pi}$ are neglected. Since the contribution from terms involving $S_{\pi\pi}$ are so substantial, it would seem reasonable to suggest that contribution from terms $S_{\pi\sigma}$ are more significant than those involving $S_{\sigma\sigma}$.

Fig. 9 also shows that the $6d_\delta/\pi_{2g}$ contributions to the delocalisation index are approximately constant across the series, with a mean value of 0.054 and a standard deviation of just 0.004. This consistency across the series suggests that, while there is a non-negligible An $6d_\delta$ contribution to covalency in these systems, its existence does not explain the variation observed in the delocalisation indices. Looking instead at the $5f_\delta/\pi_{2u}$ contributions, a trend mirroring that of the total delocalisation indices is found. In particular, there is a pronounced reduction in f-electron delocalisation in $CmCOT_2$. This can again be rationalised in terms of the antibonding π_{2u}–$5f_\delta$ orbital. Occupation of this orbital would, due to its antibonding character, be expected to reduce the covalent character of the Cm–C bond. This manifests itself in the calculated reduction in the delocalisation index.

Overall, whilst the magnitude of the $5f_\delta$ contribution is found to be smaller than the $6d_\delta$ contribution, the trend observed in the former strongly follows that of the total delocalisation indices and therefore provides strong evidence for the variation in covalency across the An series found here as having its origin in covalent $5f_\delta$ contributions to the An–COT bond.

Table 3 An–C delocalisation indices for $AnCOT_2$ (An = Th–Cm). The total number of electrons delocalised between the An centre and all sixteen carbon centres is also reported

Complex	δ(An, C)	$\sum_i \delta(\mathrm{An}, \mathrm{C}_i)$
$ThCOT_2$	0.198	3.168
$PaCOT_2$	0.218	3.488
$UCOT_2$	0.220	3.520
$NpCOT_2$	0.218	3.488
$PuCOT_2$	0.212	3.392
$AmCOT_2$	0.198	3.168
$CmCOT_2$	0.174	2.784

Summary and conclusions

In this study, the ring-metal separations of $AnCOT_2$ (An = Th–Cm) complexes were optimised at the CASPT2 level of theory, where good agreement was found with experimentally determined structural data. A trend of reducing separation was found, but this reduction was not as great as might be expected from consideration of the ionic radii of the An(IV) ions, suggesting possible increasing trivalent character as one moves across the series. Analysis of CASSCF-calculated natural orbitals was performed, and strong multiconfigurational character was found to be associated with the occupation of the $5f_\delta$ and π_{2u} orbitals. These orbitals both exhibited a strong degree of ligand–metal hybridisation and, coupled with the strong multiconfigurational character, suggested that orbital-based measures of covalency would prove ambiguous. In order to quantify covalency in an unambiguous manner, QTAIM analysis was employed. Firstly, topological properties of the electron density were considered and, in particular, the values of ρ and its Laplacian at the An–C bond critical points (BCPs) were assessed: here a significant trend in ρ was found. Initially increasing, it reached a maximum for the elements Pa–Pu before decreasing for the later actinides. An increase in ρ at the BCP is considered an indicator of increased covalent interaction, since this corresponds to an accumulation of electronic charge density in the bonding region. This analysis therefore provides evidence of enhanced covalency in the early actinides, excluding thorium. Since thorium has an empty 5f shell in its tetravalent oxidation state, it would suggest that the enhanced covalency in Pa–Pu has its origin in An 5f contributions. In order to investigate this further, integrated one- and two-electron properties were investigated, namely the atomic electron population, N(An), and the (de)localisation indices λ(An) and δ(An, C). The atomic population increased by an amount slightly greater than unity for each step across the actinide series, suggesting increased electron localisation on the An centre. There was a small deviation from this trend when considering the Cm complex, due to occupation of an antibonding orbital exhibiting a degree of ligand character. Total and orbitally resolved localisation indices were evaluated in

order to further asses the degree of electron localisation on the An centre as one traverses the actinide series. Here the degree of electron localisation derived from occupation of $6d_\delta$ and π_{2g} orbitals was found to be approximately constant across the series. The total electron localisation exhibited an increasing trend as the actinide series was traversed, and this was found to be mirrored in the variation of the contribution of the $5f_\delta$ and π_{2u} orbitals to the localisation index. Occupied nonbonding 5f orbitals were calculated to be almost entirely localised on the actinide centre. Comparison of localisation index with atomic number reveals a correlation with the expected oxidation state of the complexes.

The trend in the total delocalisation index was found to be strongly reminiscent of that found for the values of ρ at the M–C BCPs, supporting the view that increased values of ρ_{BCP} are associated with increased covalency. Again, $6d_\delta$ and π_{2g} contributions were found to be approximately constant, whereas the $5f_\delta$ and π_{2u} contributions mirrored the trend in the total delocalisation index. This therefore provides strong evidence that, while 5f contributions to covalency in these complexes are smaller in magnitude than 6d contributions, the *variation* in covalency is almost entirely accounted for by the variation in the 5f contribution.

This study demonstrates that the combination of multi-configurational quantum chemical simulations with topological analysis of the resulting electron density provides a powerful and unambiguous method for assessing and characterising covalency in high symmetry actinide complexes. That this study has been able to show that variation in covalency is almost completely accounted for by considering An 5f contributions has important implications for the design of novel ligands suitable for the challenging technological problem of An/Ln separation.

Acknowledgements

The author would like to thank the EPSRC for the award of a career acceleration fellowship (grant EP/J002208/1), UCL research computing for access to the Legion and Unity HPC facilities, the National Service for Computational Chemistry Software (NSCCS) for access to the Columbus HPC facility and the support of the Thomas Young Centre for the theory and simulation of materials.

References

1 H. H. Dam, D. N. Reinhoudt and W. Verboom, *Chem. Soc. Rev.*, 2007, **36**, 367–377.
2 Z. Kolarik, *Chem. Rev.*, 2008, **108**, 4208–4252.
3 M. P. Jensen and A. H. Bond, *J. Am. Chem. Soc.*, 2002, **124**, 9870–9877.
4 F. Lewis, M. Hudson and L. Harwood, *Synlett*, 2011, **2011**, 2609–2632.
5 M. L. Neidig, D. L. Clark and R. L. Martin, *Coord. Chem. Rev.*, 2013, **257**, 394–406.
6 N. Kaltsoyannis, *Inorg. Chem.*, 2013, **52**, 3407–3413.
7 J. R. Walensky, R. L. Martin, J. W. Ziller and W. J. Evans, *Inorg. Chem.*, 2010, **49**, 10007–10012.
8 W. W. Lukens, N. M. Edelstein, N. Magnani, T. W. Hayton, S. Fortier and L. A. Seaman, *J. Am. Chem. Soc.*, 2013, **135**, 10742–10754.
9 R. F. W. Bader, *Atoms in Molecules: A Quantum Theory*, Oxford University Press, Oxford, 1990.
10 D. Wang, W. F. van Gunsteren and Z. Chai, *Chem. Soc. Rev.*, 2012, **41**, 5836–5865.
11 A. Streitwieser and U. Müeller-Westerhoff, *J. Am. Chem. Soc.*, 1968, **90**, 7364.
12 A. Streitwieser and N. Yoshida, *J. Am. Chem. Soc.*, 1969, **91**, 7528.
13 D. F. Starks, T. C. Parsons, A. Streitwieser and N. Edelstein, *Inorg. Chem.*, 1974, **13**, 1307–1308.
14 D. G. Karraker, J. A. Stone, E. R. Jones and N. Edelstein, *J. Am. Chem. Soc.*, 1970, **92**, 4841–4845.
15 D. G. Karraker, in *Proceedings of the 4th International Transplutonium Symposium*, ed. W. Muller, North-Holland, Amsterdam, 1975, vol. II.
16 A. H. H. Chang and R. M. Pitzer, *J. Am. Chem. Soc.*, 1989, **111**, 2500–2507.
17 A. H. H. Chang, K. Zhao, W. C. Ermler and R. M. Pitzer, *J. Alloys Compd.*, 1994, **213–214**, 191–195.
18 M. Dolg, P. Fulde, H. Stoll, H. Preuss, A. Chang and R. M. Pitzer, *Chem. Phys.*, 1995, **195**, 71–82.
19 W. Liu, M. Dolg and P. Fulde, *J. Chem. Phys.*, 1997, **107**, 3584.
20 A. Kerridge, R. Coates and N. Kaltsoyannis, *J. Phys. Chem. A*, 2009, **113**, 2896–2905.
21 A. Kerridge and N. Kaltsoyannis, *J. Phys. Chem. A*, 2009, **113**, 8737–8745.
22 A. Kerridge, *Dalton Trans.*, 2013, **42**, 16428–16436.
23 B. Roos, P. R. Taylor and P. E. M. Siegbahn, *Chem. Phys.*, 1980, **48**, 157–173.
24 G. Karlström, R. Lindh, P.-Å. Malmqvist, B. O. Roos, U. Ryde, V. Veryazov, P.-O. Widmark, M. Cossi, B. Schimmelpfennig, P. Neogrady and L. Seijo, *Comput. Mater. Sci.*, 2003, **28**, 222–239.
25 F. Aquilante, L. D. E. Vico, N. Ferré, G. Ghigo, P.-Å. Malmqvist, P. Neogrády, T. B. Pedersen, M. P. Nák, M. Reiher, B. O. Roos, L. Serrano-andrés, M. Urban, V. Veryazov and R. Lindh, *J. Comput. Chem.*, 2010, **31**, 224–247.
26 B. O. Roos, R. Lindh, P.-Å. Malmqvist, V. Veryazov and P.-O. Widmark, *J. Phys. Chem. A*, 2004, **108**, 2851–2858.
27 B. O. Roos, R. Lindh, P.-A. Malmqvist, V. Veryazov, P.-O. Widmark and A. C. Borin, *J. Phys. Chem. A*, 2008, **112**, 11431–11435.
28 B. O. Roos, R. Lindh, P.-Å. Malmqvist, V. Veryazov and P.-O. Widmark, *Chem. Phys. Lett.*, 2005, **409**, 295–299.
29 K. Anderson, P.-Å. Malmqvist, B. O. Roos, A. J. Sadlej and K. Wolinskit, *J. Phys. Chem.*, 1990, 5483–5488.
30 T. A. Keith, *AIMAll (Version 13.05.06), TK Gristmill Software*, Overl. Park KS, USA, 2013.
31 T. Lu and F. Chen, *J. Comput. Chem.*, 2012, **33**, 580–592.
32 A. E. Clark, J. L. Sonnenberg, P. J. Hay and R. L. Martin, *J. Chem. Phys.*, 2004, **121**, 2563–2570.

33 L. Petit, C. Adamo and P. Maldivi, *Inorg. Chem.*, 2006, **45**, 8517–8522.
34 A. Avdeef, K. N. Raymond, K. O. Hodgson and A. Zalkin, *Inorg. Chem.*, 1972, **11**, 1083–1088.
35 D. J. A. De Ridder, J. Rebizant, C. Apostolidis, B. Kanellakopulos and E. Dornberger, *Acta Crystallogr., Sect. C: Cryst. Struct. Commun.*, 1996, **52**, 597–600.
36 R. D. Shannon, *Acta Crystallogr., Sect. A: Cryst. Phys., Diffr., Theor. Gen. Crystallogr.*, 1976, **32**, 751–767.
37 P. Löwdin, *Phys. Rev.*, 1955, **376**, 1474–1489.
38 M. W. Schmidt and M. S. Gordon, *Annu. Rev. Phys. Chem.*, 1998, **49**, 233–266.
39 A. Streitwieser, D. Dempf, G. N. La Mar, and N. Edelstein, 1971, **93**, 7343–7344.
40 K. D. Warren, *Inorg. Chem.*, 1975, **14**, 3095–3103.
41 J. P. Clark and J. C. Green, *Dalton Trans.*, 1977, 505–508.
42 P. M. Boerrigter, E. J. Baerends and J. G. Snijders, *Chem. Phys.*, 1988, **122**, 357–374.
43 J. G. Brennan, J. C. Green, and C. M. Redfern, 1989, **111**, 2373–2377.
44 R. Coates, M. Coreno, M. DeSimone, J. C. Green, N. Kaltsoyannis, A. Kerridge, N. Narband and A. Sella, *Dalton Trans.*, 2009, 5943–5953.
45 A. Kerridge and N. Kaltsoyannis, *C. R. Chim.*, 2010, **13**, 853–859.
46 R. F. W. Bader, *J. Phys. Chem. A*, 2009, **113**, 10391–10396.
47 I. Kirker and N. Kaltsoyannis, *Dalton Trans.*, 2011, **40**, 124–131.
48 A. M. K. Müller, *Phys. Lett. A*, 1984, **105**, 446–452.
49 F. Feixas, J. Vandenbussche, P. Bultinck, E. Matito and M. Solà, *Phys. Chem. Chem. Phys.*, 2011, **13**, 20690–20703.

